Proof-of-Principle Experiment on the Dynamic Shell Formation for Inertial Confinement Fusion

I. V. Igumenshchev, W. Theobald,* C. Stoeckl, R. C. Shah, D. T. Bishel,† V. N. Goncharov,* M. J. Bonino, E. M. Campbell, L. Ceurvorst, D. A. Chin,† T. J. B. Collins, S. Fess, D. R. Harding, S. Sampat, N. R. Shaffer, A. Shvydky, E. A. Smith,† W. T. Trickey, and L. J. Waxer
Laboratory for Laser Energetics, 250 East River Road, Rochester, New York 14623-1212, USA

A. Colaïtis and R. Liotard
Centre Lasers Intenses et Applications, UMR 5107, 351 Cours de la libération, 33400 Talence, France

P. J. Adrian
Plasma Science and Fusion Center, MIT, Boston, MA, USA

S. Atzeni, F. Barbato, and L. Savino
Dipartimento SBAI, Università degli Studi di Roma "La Sapienza", Roma, Italy

N. Alfonso, A. Haid, and Mi Do
General Atomics, San Diego, CA, USA
(Dated: July 11, 2023)

In the dynamic-shell (DS) concept [Goncharov *et al.*, Phys Rev. Lett. **125**, 065001 (2020)] for laser-driven inertial confinement fusion the deuterium-tritium fuel is initially in the form of a homogeneous liquid inside a wetted-foam spherical shell. This fuel is ignited using a conventional implosion, which is preceded by a initial compression of the fuel followed by its expansion and dynamic formation of a high-density fuel shell with a low-density interior. This letter reports on a scaled-down, proof-of-principle experiment on the OMEGA laser demonstrating, for the first time, the feasibility of DS formation. A shell is formed by convergent shocks launched by laser pulses at the edge of a plasma sphere, with the plasma itself formed as a result of laser-driven compression and relaxation of a surrogate plastic-foam ball target. Three x-ray diagnostics, namely, 1-D spatially resolved self-emission streaked imaging, 2-D self-emission framed imaging, and backlighting radiography, have shown good agreement with the predicted evolution of the DS and its stability to low Legendre mode perturbations introduced by laser irradiation and target asymmetries.

The dynamic-shell (DS) concept [1] in inertial confinement fusion (ICF) uses as fuel a cryogenic liquid-sphere target of deutrium–tritium (DT) that has the potential to meet the goal of low-cost mass production for an inertial fusion energy (IFE) prospect [2, 3]. This target is dynamically shaped into a shell by the application of a carefully designed train of laser pulses and then ignited utilizing the conventional hot-spot ignition scheme [3].

This Letter describes results of a proof-of-principle experiment on the OMEGA laser [4] that demonstrates, for the first time, the feasibility of DS formation in direct laser-driven implosions using a scaled-down experimental setup with surrogate plastic-foam ball targets and laser pulses modified to satisfy the limitations of the OMEGA laser in the available energy ($\lesssim$20 kJ) and the pulse duration ($\leq$4 ns). The strong megabar shocks that are produced in this experiment instantaneously transform the foam material to an uniform high-temperature plasma justifying the use of these targets as surrogates for liquid-DT targets. The surrogate targets driven by the modified laser pulses undergo the same evolution stages as cryogenic targets in DS ignition designs as described below, but missing fusion reactions in the hot spot at the final stage.

Dynamic shell designs with significant gain ($G \sim 100$) require low-adiabat ($\alpha \lesssim 2$) imploding shells, with G the ratio of fusion energy to incident laser energy and the adiabat α the ratio of the plasma pressure to the Fermi-degenerated pressure. Such shells can be formed either with an appropriately time-shaped continuous pulse or with a sequence of short picket pulses ($\sim$200- to 500-ps duration). Pickets have the advantage of producing more stable implosions as discussed in Ref. [1]. A typical 1-D simulation of a DS design with significant gain using the multidimensional radiation-hydrodynamic code *ASTER* [5] is illustrated in Fig. 1, which shows a "shock diagram" (a plot of log-density evolution) in color scale. This design uses a 1.3-MJ laser pulse, which is shown by the blue line, and a 3280-μm-diameter cryogenic target consisting of DT liquid within an outer 420-μm-thick wetted-foam spherical layer with a density of 0.22 and 0.33 g/cm^3, respectively. The pulse is about 210-ns long and consists

* Also at Department of Mechanical Engineering, University of Rochester, Rochester, New York 14623, USA
† Also at Department of Physics and Astronomy, University of Rochester, Rochester, New York 14623, USA

of 12 pickets and a final ramp compression pulse.

The DS formation and fuel ignition are accomplished in four evolution stages. In the first stage, the target is compressed using shocks launched by the first three pickets of the pulse (see Fig. 1). Trajectories of these shocks are seen in Fig. 1 as the three high-contrast trajectories in the color-scaled image before merging and approaching the center at $t = 63$ ns. The corresponding bounce of these shocks from the center results in a blast wave and an expansion of the target mass (second stage). During the third stage, a sequence of eight shocks, launched by the next eight pickets starting at $t = 50$ ns, decelerate the expanding cloud and form a dense shell. In the fourth stage, the last picket at $t = 188$ ns and the following ramp-compression pulse drive a low-adiabat implosion, resulting in ignition with $G = 100$.

The DS concept has a number of advantages over other ICF concepts. These advantages include, among others, the relative simplicity of fabrication of cryogenic DT-liquid ball targets (since no forming of a DT-ice shell is required) with a potentially smoother target surface with fewer defects seeding perturbations. Such targets are appropriate for mass production required for commercial IFE plants. The large parameter space of DS designs introduces the flexibility of varying the convergence ratio (the ratio of the maximum shell radius to minimum shell radius at stagnation) of imploding shells [1] and varying their stability properties. The DS concept is compatible with the central hot-spot and shock-ignition approaches [6].

On the downside, the DS concept requires complicated long-duration laser pulses that are not available on current systems (but can be available on future systems, e.g., StarDriver [7]) These pulses result in complicated target dynamics affecting the evolution of various perturbations, caused, e.g., by target imperfections, target offset, laser beam pointing, and laser imprint. The formation of the DS and its sensitivity to such perturbations should be addressed both experimentally and by systematic simulation studies.

The OMEGA experiment used laser pulses, in which

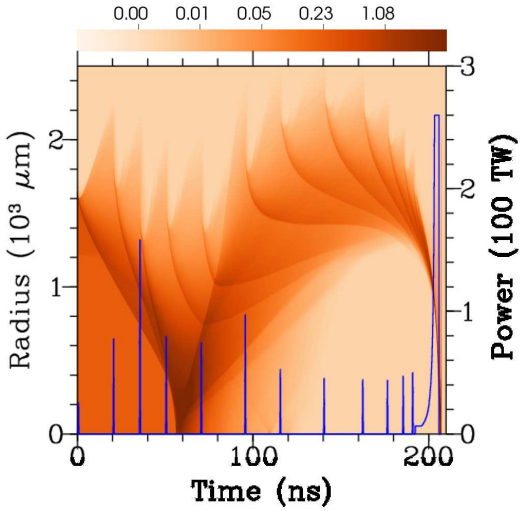

FIG. 1. Laser power history (blue line) for an ignition DS design using the target described in the text. The graded color image shows the log-density evolution (a "shock diagram") from 1-D simulations. The upper bar indicates the log-density scale in g/cm^3. The density interfaces indicate spherical convergent or divergent shock waves.

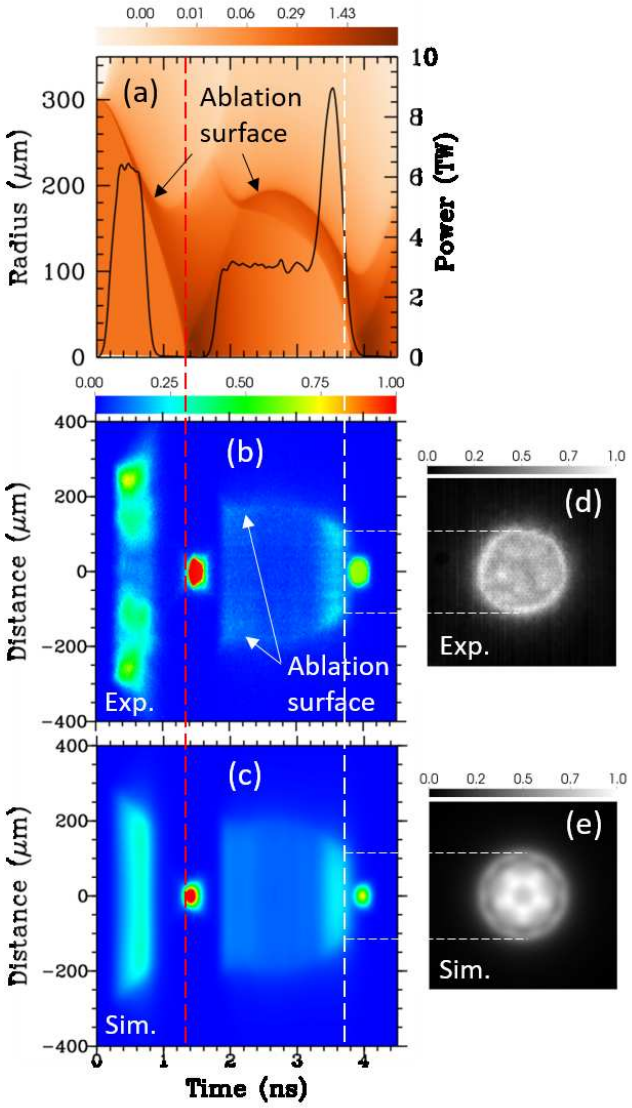

FIG. 2. (a) Laser power history (black line) and simulated shock diagram (graded color image) for OMEGA shot 105251 using the target shown in Fig. 3(a). For the same shot: (b) and (c) streaked measured and simulated self-emission radiographs, respectively; (d) and (e) framing camera measured and simulated radiographs, respectively. The upper bar at (a) indicates the log-density scale in g/cm^3, and such bars at (b)–(e) indicate the linear scale of relative fluence.

the compression and shell-forming pickets of the ignition design (Fig. 1) are replaced with relatively high-power continuous pulses. This results in a DS with higher adiabat ($\alpha \gtrsim 10$) than it would be necessary for a high-gain design. Such a DS is less suceptible to the high Legendre mode ($\ell \gtrsim 30$) perturbation growth [3]. An example of the laser pulse of shot 105251 is shown in Fig. 2(a) by the black line. It consisted of two square pulses of about 0.5- and 2-ns duration, respectively, with a 1-ns gap between them. The second pulse ends with a power spike, which is used to additionally compress the DS during its implosion. The total pulse energy was 11.2 kJ and the duration was about 4 ns. Sixty laser beams were focused on target using SG5-650 distributed phase plates [8], each of which produces a spot with an order-4.2 super-Gaussian profile with $R_{\rm b} = 337$ μm, where $R_{\rm b}$ is the radius encirculating 95% of the beam energy. The beams were smoothed by polarization smoothing [9] and smoothing by spectral dispersion [10] at 0.3-THz bandwidth and three color cycles [11].

The ball targets were made of a CH foam with a mass density of $\sim$0.130 g/cm^3 and an outer diameter of $\sim$605 μm [see Fig. 3(a)]. Each target was attached to a solid plastic (CH) stump of 50 μm in diameter and 200 μm in length and a density of $\sim$1.1 g/cm^3. The target and stump were printed simultaneously using the two-photon polymerization (2PP) technique [12]. The target was mounted on a stalk (silicon-carbon fiber of 17 μm in diameter), which was glued to the stump [Fig. 3(a)]. The foam is built using the body-centered-cubic lattice structure. Each lattice node is connected to others by eight fibers of about 8 μm in length, each having an approximately elliptical cross section with dimensions of about 2.3×0.7 μm. These fibers are arranged in space to have the minimum projected thickness [$\sim$0.7 μm, see Fig. 3(b)] in the direction of the stalk and the maximum [$\sim$2.3 μm, see Fig. 3(c)] in the perpendicular directions. This foam asymmetry is likely the reason of an observed mode ℓ=2 implosion asymmetry discussed later.

Figure 2(a) illustrates the DS evolution stages (compression, expansion, shell formation, and implosion) in shot 105251 showing the shock diagram, which was simulated with *ASTER* considering foam as a continuous medium at an equivalent volume-averaged density. The first square pulse launches a shock that initially compresses the target. This shock bounces from the center at $t = 1.4$ ns, forming a blast wave and resulting in expansion of the compressed target mass. The second square pulse, which starts at $t = 1.8$ ns, decelerates the expanding plasma and forms a dense shell. The outer shell radius, which is defined as the radius of the ablation surface and seen as a density interface in Fig. 2(a), initially reduces to about 180 μm at 2.15 ns, then increases to reach about 200 μm at 2.8 ns, and then decreases again approaching the minimum of about 120 μm at 4.0 ns. A dense shell of outer radius of about 150 μm is formed at $t = 3.8$ ns.

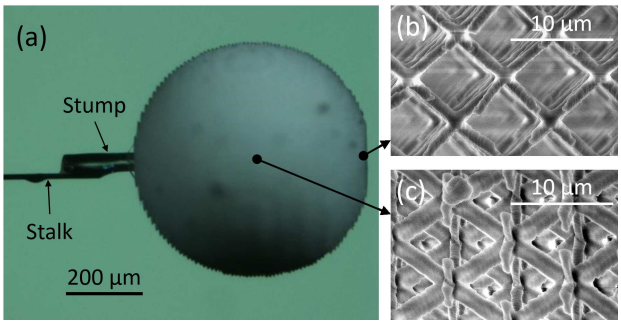

FIG. 3. (a) Surrogate foam-ball target mounted on a stalk. Foam lattice imaged (b) in the direction closely aligned with the stalk and (c) in the perpendicular direction.

The experiments employed three x-ray diagnostics to probe the DS formation. These include a streaked self-emission 1-D imaging [13], framed self-emission 2-D imaging [14], and backlighting radiography [15]. Figure 2(b) shows the streaked data obtained in shot 105251. The streak camera collects x rays at around 1 keV. These data compared with a synthetic streak image in Fig. 2(c) from post-processing 1-D *ASTER* simulations, which include cross-beam energy transfer (CBET) [16] and assume Spitzer–Härm heat conduction [17]. Nearly identical streak images were obtained using hydrodynamic simulations with the code *DUED* [18] (using the sharp-cutoff flux-limiter [3] of 0.07 and omitting CBET, but reducing laser power by about 15% to account for CBET losses) and a similar postprocessor. Figures 2(b) and 2(c) show vertically extended bright spots between $t = 0$ and 1 ns, corresponding to the emission from the target surface caused by the leading square laser pulse. The discrepancy in the shape of the measured and simulated spots might be attributed to high-z debris unintentionally collected and randomly distributed on the outer surface of targets during their handling, and not accounted for in the simulations. Several tens of such several-micron-in-size debris were found on each target [e.g., seen as dark spots on the ball surface in Fig. 3(a)]. They can be avoided by improved foam manufacturing and handling techniques.

The bright red spot at $t \approx 1.5$ ns in Fig. 2(b) is the signature of the emission from the first shock bounce [see Fig. 2(a); the vertical red dashed line indicates the time of the bounce]. The onset of this emission is accurately reproduced in simulations [see Fig. 2(c)] within the uncertainty of the absolute timing of the diagnostic ($\sim$10 ps). These results are in good agreement with *ASTER* simulations using the 3-D ray-trace code *IFRIIT* [19] and a recently developed solid-to-plasma transition model [20] for foams, including the effect of shinethrough, which did not show significant influence on shock timing and areal-density evolution for the considered high-adiabat design.

The next bright region in Fig. 2(b) starts with the beginning of the second square laser pulse at $t = 1.8$ ns and corresponds to the emission from the ablation surface of the decelerating expanding plasma. The top and bottom rims of this region represent the ablation surface trajec-

tory, which is observed in the shock diagram in Fig. 2(a) as the outer contrast-density line. The synthetic streak in Fig. 2(c) faithfully reproduces the measured trajectory. Note the brighter and dimmer vertical strips in the bright region between $t \simeq 1.8$ and 3.8 ns in both Figs. 2(b) and 2(c), which appearence correlate with variation of the incident laser power.

The second bright spot at $t \approx 4.0$ ns [green-yellow spot in Figs. 2(b)] is the signature of the collapse of the dense shell that is seen in Fig. 2(a). Note that simulations predict the onset of this spot by about 50 ps later [see Fig. 2(c)].

Framing-camera images, with a spatial resolution of $\sim$20 μm and $\sim$30-ps time averaging, indicate the DS formation during the implosion stage. Figure 2(d) shows a self-emission x-ray image of the DS target in shot 105251 at $t = 3.75 \pm 0.05$ ns. The vertical white dashed line in Figs. 2(a)–2(c) indicates $t = 3.75$ ns for convenience. The outer bright circular rim and the dim region inside it in Fig. 2(d) are because of limb brightening caused by emission of the high-temperature ablation plasma. In addition, emission from the opposite (vs. face-on) side of the target is screened by the opaque dense shell making the dim region dimmer. Figure 2(d) also reveals five almost symmetrical bright spots in the dim region indicating mode ℓ=10 perturbations in the imploding target.

Nominal 3-D *ASTER* simulations reproduce the outer bright rim and inner dim region similar to those in Fig. 2(d), but do not reproduce the five-spot structure, showing instead a brighter central region caused by leaked through the opaque shell radiation from the hot plasma inside the shell. The five-spot structure was, however, reproduced in simulations, which artificially supress the lateral heat flux ($\times$0.05) resulting in enhanced perturbations at the ablation surface induced by the OMEGA beam illumination pattern [see Fig. 2(e)]. This spot structure closely reproduces the symmetry of the structure in Fig. 2(d) with spots themselve appear at depressions (with reduced optical depth) on the ablation surface. The symmetry of the structure is explained by the symmetry of the OMEGA beam-port configuration when viewing through the center of the pentagon formed by the ports. Further investigation of the reason of the enhanced perturbations is required.

Backlighting radiography [15] used an infrared (1053-nm) 20-ps, 1.5-kJ short-pulse beam from the OMEGA EP laser [21] that was focused with an intensity of 3×10^{16} W/cm^2 onto a Si foil target with a CH side shield [22] for producing the Si He$_\alpha$ line emission at 1.865 keV that transmits through the shell target. This target was imaged by a shaped Bragg crystal onto a single-strip x-ray framing camera with a spatial resolution of $\sim$15 μm. Figure 4(a) shows a radiographic image in shot 105249 that was obtained by firing the backlighting beam at $t = 4.0 \pm 0.03$ ns, corresponding to the time of stagnation of the imploding shell. Imaging was started at $t = 3.8 \pm 0.2$ ns and integrated over about 400 ps, so that the center bright spot, which is caused by the shell

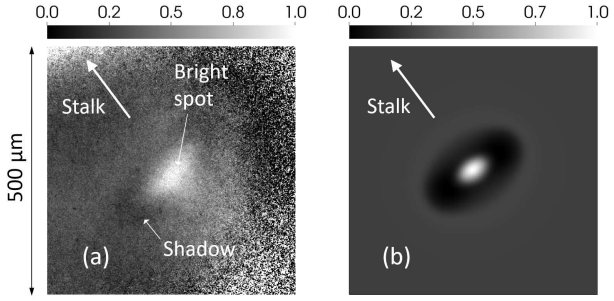

FIG. 4. (a) Measured and (b) simulated backlighting radiographs at the moment of stagnation of the dense shell for OMEGA shot 105249. The center bright spot corresponds to emission of hot-spot plasma resulting from the collapse of the shell. The dark ellipse surrounding the spot is a shadow of the shell. The upper bars indicate the linear scale of relative fluence.

collapse and observed in Fig. 2(b), is observed in this radiograph as well. The shadow of the stagnated shell surrounding the central bright spot in Fig. 4(a) demonstrate a large mode ℓ=2. The shell takes an oblate spheroid shape with the aspect ratio of about 2 and with the minor axis closely aligned with the stalk. Note that these spheroidal perturbations of DS continuously grow in time and, in principal, should be observed at earlier time in Fig. 2(d), but at smaller amplitude. To find them at that time, one must employ the full 3-D reconstruction technique [23] requiring multiple imaging diagnostics that were not employed in these experiments. Future experiments will include such diagnostics.

Three-dimensional *ASTER-IFRIIT* simulations suggest that the effects of stalks, target offsets (typically $\lesssim$5 μm), and target ellipticity (typically $\lesssim$2% peak-to-valey in radius) and typical errors in mispointing ($\lesssim$10 μm) and power balance ($\lesssim$5%) of the OMEGA laser beams are insufficient to explain the observed implosion asymmetry. These simulations also suggest that such an asymmetry can result from a significantly nonuniform compression of the foam target during the initial compression stage. As an example, Fig. 4(b) shows a synthetic radiograph of a stagnating shell from simulations of shot 105249 assuming a temporally applied (from $t = 0$ to 1 ns) mode ℓ=2 perturbation in beam power with $\sigma_{\rm rms} = 20\%$ with more power supplied to beams perpendicular to the stalk. The shadow in this radiograph reasonably well reproduces the asymmetry of the shadow in Fig. 4(a), including its alignment with the stalk. The assumed perturbations can be explained by the effects of foam structural asymmetry that were discussed earlier. In such a case, the foam target, which is more porous along the stalk, is compressed faster by shocks in the direction perpendicular to the stalk. The seeming disagreement between this compression leading to a prolate shape and the oblate shape of the shell in Figs. 4(a) and 4(b) is explained by a phase inversion of the mode ℓ=2 perturbation during the shock bounce at $t = 1.4$ ns.

In summary, the proof-of-principle experiment on the OMEGA laser has demonstrated, for the first time, the feasibility of DS formation in the scaled-down setup using surrogate plastic-foam ball targets. Three x-ray diagnostics evidenced the DS formation and showed good agreement with synthetic x-ray radiographs obtained by post-processing the results of 3-D radiation-hydrodynamic *ASTER-IFRIIT* simulations. The developed DS's show good stability to low ℓ-mode perturbations including mode ℓ=1 perturbations caused by mount stalks and target offsets, mode ℓ=2 asymmetry possibly developed due to the asymmetric foam structure, and mode ℓ=10 perturbations from OMEGA beams. Good agreement in timing of measured and predicted x-ray flashes from shock bounce and shell collape indicates the plausibility of modeling foams as a continuous medium at an equivalent volume-averaged density in agreement with earlier studies [24]. Further work is required to reproduce and explain the observed mode ℓ=10 perturbations in imploding shells.

ACKNOWLEDGMENTS

This material is based upon work supported by the Department of Energy National Nuclear Security Administration under Award Number DE-NA0003856 and ARPA-E BETHE Grant No. DE-FOA-0002212. The experiment was conducted at the Omega Laser Facility at the University of Rochesters Laboratory for Laser Energetics with the beam time through the Laboratory Basic Science (LBS) program. The work of P. J. A. was supported by DE-NA0003868 and DE-NA0003960. The work of S. A., F. B. and L. S. (Rome Sapienza) was supported by the European Union via the Euratom Research and Training Programme (Grant Agreement No 101052200 EUROfusion), within the framework of the Enabling Research Project: ENR-IFE.01.CEA "Advancing shock ignition for direct-drive inertial fusion".

[1] V. N. Goncharov, I.V. Igumenshchev, D. R. Harding, S.F.B. Morse, S. X. Hu, P. B. Radha, D. H. Froula, S. P. Regan, T.C. Sangster, and E. M. Campbell, Novel hot-spot ignition designs for inertial confinement fusion with liquid-deuterium-tritium spheres, Phys. Rev. Lett. **125**, 065001 (2020).

[2] J. J. Duderstadt and G. A. Moses, *Inertial Confinement Fusion*, (John Wiley & Sons, New York 1982), pp. 306-342.

[3] S. Atzeni and J. Meyer-ter-Vehn, *The Physics of Inertial Fusion: Beam Plasma Interaction, Hydrodynamics, Hot Dense Matter*, 1st ed., International Series of Monographs on Physics, vol. 125 (Oxford University Press, Oxford, 2004), p. 43.

[4] T. R. Boehly, D. L. Brown, R. S. Craxton, R. L. Keck, J. P. Knauer, J. H. Kelly, T. J. Kessler, S. A. Kumpan, S. J. Loucks, S. A. Letzring *et al.*, Initial performance results of the OMEGA Laser System, Opt. Commun. **133**, 495 (1997).

[5] I. V. Igumenshchev, V. N. Goncharov, F. J. Marshall, J. P. Knauer, E. M. Campbell, C J. Forrest, D. H. Froula, V. Yu. Glebov, R. L. McCrory, S. P. Regan *et al.*, Three-dimensional modeling of direct-drive cryogenic implosions on OMEGA, Phys. Plasmas **23**, 052702 (2016).

[6] R. Betti, C. Zhou, K. S. Anderson, L. J. Perkins, W. Theobald, and A. A. Solodov, Shock Ignition of Thermonuclear Fuel with High Areal Density, Phys. Rev. Lett. **98**, 155001 (2007).

[7] D. Eimerl, E. M. Campbell, W. F. Krupke, J. Zweiback, W. L. Kruer, J. Marozas, J. Zuegel, J. Myatt, J. Kelly, D. Froula, and R. L. McCrory, StarDriver: a flexible laser driver for inertial confinement fusion and high energy density physics, Journal of Fusion Energy **33**, 476 (2014).

[8] W. Theobald, D. Cao, R. C. Shah, C. A. Thomas, I. V. Igumenshchev, K. A. Bauer, R. Betti, M. J. Bonino, E. M. Campbell, A. R. Christopherson *et al.*, Enhanced laser-energy coupling with small-spot distributed phase plates (SG5-650) in OMEGA DT cryogenic target implosions, Phys. Plasmas **29**, 012705 (2022).

[9] J. E. Rothenberg, Polarization beam smoothing for inertial confinement fusion, J. Appl. Phys. **87**, 3654 (2000).

[10] S. Skupsky, R. W. Short, T. Kessler, R. S. Craxton, S. Letzring, and J. W. Soures, Improved laser-beam uniformity using the angular dispersion of frequency-modulated light, J. Appl. Phys. **66**, 3456 (1989).

[11] S. P. Regan, J. A. Marozas, R. S. Craxton, J. H. Kelly, W. R. Donaldson, P. A. Jaanimagi, D. Jacobs-Perkins, R. L. Keck, T. J. Kessler, D. D. Meyerhofer *et al.*, Performance of 1-THz-bandwidth, two-dimensional smoothing by spectral dispersion and polarization smoothing of high-power, solid-state laser beams, J. Opt. Soc. Am. B **22**, 998 (2005).

[12] S. Maruo, O. Nakamura, and S. Kawata, Three-dimensional microfabrication with two-photon-absorbed photopolymerization, Opt. Lett. **22**, 132 (1997).

[13] S. Ressel, J. J. Ruby, G. W. Collins, and J. R. Rygg, Density reconstruction in convergent high-energy-density systems using x-ray radiography and Bayesian inference, Phys. Plasmas **29**, 072713 (2022).

[14] D. T. Michel, C. Sorce, R. Epstein, N. Whiting, I. V. Igumenshchev, R. Jungquist, and D. H. Froula, Shell trajectory measurements from direct-drive experiments, Rev. Sci. Instrum. **83**, 10E530 (2012).

[15] C. Stoeckl, R. Epstein, R. Betti, W. Bittle, J. A. Delettrez, C. J. Forrest, V. Yu. Glebov, V. N. Goncharov, D. R. Harding, I. V. Igumenshchev *et al.*, Monochromatic backlighting of direct-drive cryogenic DT implosions on OMEGA, Phys. Plasmas **24**, 056304 (2017).

[16] I. V. Igumenshchev, D. H. Edgell, V. N. Goncharov, J. A. Delettrez, A. V. Maximov, J. F. Myatt, W. Seka, A. Shvydky, S. Skupsky, and C. Stoeckl, Crossed-beam energy transfer in implosion experiments on OMEGA, Phys. Plasmas **17**, 122708 (2010).

[17] L. Spitzer, Jr. and R. Härm, Transport phenomena in a completely ionized gas, Phys. Rev. **89**, 977 (1953).

[18] S. Atzeni, A. Schiavi, F. Califano, F. Cattani, F. Cornolti, D. Del Sarto, T. V. Liseykina, A. Macchi, and F. Pegoraro, Fluid and kinetic simulation of inertial confinement fusion plasmas, Comput. Phys. Commun. **169**, 153 (2005).

[19] A. Colaïtis, I. Igumenshchev, J. Mathiaud, and V. Goncharov, Inverse ray tracing on icosahedral tetrahedron grids for non-linear laser plasma interaction coupled to 3D radiation hydrodynamics, J. Comput. Phys. **443**, 110537 (2021).

[20] A. Pineau, B. Chimier, S. X. Hu, and G. Duchateau, Modeling the electron collision frequency during solid-to-plasma transition of polystyrene ablator for direct-drive inertial confinement fusion applications, Phys. Plasmas **27**, 092703 (2020).

[21] L. J. Waxer, D. N. Maywar, J. H. Kelly, T. J. Kessler, B. E. Kruschwitz, S. J. Loucks, R. L. McCrory, D. D. Meyerhofer, S. F. B. Morse, C. Stoeckl *et al.*, High-energy petawatt capability for the OMEGA laser, Opt. Photonics News **16**, 30 (2005).

[22] C. Stoeckl, M. Bonino, C. Mileham, S. Regan, W. Theobald, T. Ebert, and S. Sander, Optimization of a short-pulse-driven Si He_α soft x-ray backlighter, High Energy Density Physics **41**, 100973 (2021).

[23] D.T. Michel, I.V. Igumenshchev, A.K. Davis, D.H. Edgell, D.H. Froula, D.W. Jacobs-Perkins, V.N. Goncharov, S.P. Regan, A. Shvydky, and E.M. Campbell, Subpercent-Scale Control of 3D Low Modes of Targets Imploded in Direct-Drive Configuration on OMEGA, Phys. Rev. Lett. **120**, 125001 (2018).

[24] Y. Aglitskiy, A. L. Velikovich, M. Karasik, A. J. Schmitt, V. Serlin, J. L. Weaver, J. Oh, S. P. Obenschain, and K. R. Cochrane, Absolute Hugoniot measurements for CH foams in the 29 Mbar range, Phys. Plasmas **25**, 032705 (2018).